Available online at www.sciencedirect.com
ScienceDirect
Ceramics International 35 (2009) 887–896
CERAMICS INTERNATIONAL
www.elsevier.com/locate/ceramint

Conduction model of oxide ions at grain boundary of solid electrolyte

Yoshihiro Hirata *, Akihiro Hara

Department of Advanced Nanostructured Materials Science and Technology, Kagoshima University, 1-21-40 Korimoto, Kagoshima 890–0065, Japan

Received 10 December 2007; received in revised form 18 February 2008; accepted 10 March 2008
Available online 1 July 2008

Abstract

A flux of oxide ions of solid electrolyte at a grain boundary was correlated to the difference of activity (a_r) of oxide ions within two adjacent grains with different curvature at a given electric field. The flux leads to two types of conductivity: increased conductivity ($\sigma_i(+)$) and decreased conductivity ($\sigma_i(-)$) with decreasing grain size. Both the conductivities reach a maximum or minimum value at $r = r_c$ where $a_r = 1$ (for $r > 0$) or $a_r = a_0^2$ (for $r < 0$, a_0 is the activity for $r = \infty$). In the grain size range of $r_c > r$, $\sigma_i(+)$ or $\sigma_i(-)$ is independent of grain size. As a result, total conductivity $\sigma(t)$ ($=(\sigma_i(+) + \sigma_i(-))/2$) is expressed as a curve of second degree of reciprocal grain size ($1/r$) and reaches a maximum value at $r = r_c$. The dependence of activation energy of conductivity on the grain size is theoretically small in the wide grain size range of $\infty > r > r_c$. The derived theory was compared with the experimental data of the grain boundary conductivity of sintered Gd-doped ceria. A good agreement was recognized between the theory and experiments for the dependence of conductivity and activation energy on grain size.

Keywords: A. Hot pressing; B. Grain size; C. Ionic conductivity; E. Fuel cells

1. Introduction

Rare-earth-doped ceria (shorten as RDC) shows a higher oxide ion conductivity than yttria-stabilized zirconia at 500–1000 °C in air. This favorable property enables to use RDC as an electrolyte of solid oxide fuel cell [1–4]. In our previous papers [5–10], we measured the oxide ion conductivity of high purity RDC (R = Yb, Y, Sm, Gd, Nd, or La) in air at 300–800 °C and electronic conductivity in an oxygen pressure range from 10^5 to 10^{-32} Pa at 500–840 °C by Hebb–Wagner method. The influence of doped rare-earth oxide on the conductivity and activation energy for the diffusion of oxide ions was relatively small. The conductivity as a function of ionic radius of dopant was highest at about 0.105 nm of Sm or Gd. The grain boundary conductivity of RDC is greatly small as compared with the bulk conductivity [5,7,11,12]. However, the total conductivity is dominated by the bulk conductivity at a high temperature because of the small volume fraction of thin grain boundary layers. Furthermore, it was found that the transference number of oxide ion of La-doped ceria increases with a decrease of heating temperature and is close to unity by 10^{-15} Pa of oxygen partial pressure at 500 °C [10]. The above results suggest it is possible to use RDC as a solid electrolyte of SOFC facing both air and fuel of low oxygen partial pressure at a relatively low temperature. When the heating temperature of RDC is reduced, the fraction of resistivity of the diffusion of oxide ions at grain boundary to the total resistivity increases [5]. That is, understanding and enhancement of grain boundary conductivity are important for a low temperature SOFC. On the other hand, several papers report the enhancement of oxide ion conductivity of RDC with decreasing grain size [12–14]. These phenomena are attractive to increase the conductivity at a low temperature but no clear mechanism has been proposed. On the other hand, Ou et al. [15] observed the segregation of cations and oxygen vacancy ordering in nanosized domains of rare-earth-doped ceria grains (Sm, Dy, Y and Yb, 25 at%). This ordering of oxygen vacancy leads to the decrease of oxide ion conductivity. Based on the above background, we have analyzed the relationship between grain boundary conductivity and grain size of RDC based on the thermodynamics of solids. The derived theory succeeded in explaining the experimentally measured dependence of grain boundary conductivity on grain size for Gd-doped ceria (GDC). The flux of oxide ions through a grain boundary is derived from the difference of activity of oxide ions within two adjacent grains in the latter sections.

* Corresponding author. Tel.: +81 99 285 8325; fax: +81 99 257 4742.
E-mail address: hirata@apc.kagoshima-u.ac.jp (Y. Hirata).

0272-8842/$34.00
doi:10.1016/j.ceramint.2008.03.007

2. Difference of chemical potential between grains of different sizes

Fig. 1 shows a model structure for the migration of oxide ions between two adjacent single crystal grains of GDC. When 1 mol of oxide ions in grain 1 moves though the grain boundary to grain 2, the free energy change of each grain is represented by chemical potential (μ_i) by Eq. (1),

$$\mu_i = \left(\frac{\partial G}{\partial n_i}\right)_{\mathrm{T,P,n_j}} \tag{1}$$

The decreased (for grain 1) and increased (for grain 2) volumes due to the migration of oxide ions give the following relations using Eq. (1) [16],

$$-\frac{\mathrm{d}G_1}{\mathrm{d}V} = \frac{\mu_1 \mathrm{d}n}{\mathrm{d}V} = \frac{\mu_1}{(\mathrm{d}V/\mathrm{d}n)} = \frac{\mu_1}{\upsilon} \tag{2}$$

$$\frac{\mathrm{d}G_2}{\mathrm{d}V} = \frac{\mu_2 \mathrm{d}n}{\mathrm{d}V} = \frac{\mu_2}{(\mathrm{d}V/\mathrm{d}n)} = \frac{\mu_2}{\upsilon} \tag{3}$$

where υ is the volume of oxide ions of 1 mol. The total energy ($\mathrm{d}G = \mathrm{d}G_1 + \mathrm{d}G_2$) is expressed by the difference of the chemical potential of both the grains [16].

$$\frac{\mathrm{d}G}{\mathrm{d}V} = \frac{\mu_2 - \mu_1}{\upsilon} = \frac{\Delta\mu}{\upsilon} \tag{4}$$

This type of material transport between two grains can be seen in the grain growth phenomenon in a sintered microstructure containing different grain sizes and curvature. Of course, when the volumes of input and output mass are same in one grain, no charge in grain size occurs. On the other hand, $\mathrm{d}G$ is related to the change of surface area of two grains by Eq. (5),

$$\mathrm{d}G = \gamma \mathrm{d}A_1 + \gamma \mathrm{d}A_2 \tag{5}$$

where γ is the surface energy. Since $\mathrm{d}V$ ($=4\pi r^2 \mathrm{d}r$) is related to $\mathrm{d}A$ ($=8\pi r \mathrm{d}r$) by $\mathrm{d}A = 2\mathrm{d}V/r$ (r: radius of grain), Eq. (5) results in Eq. (6).

$$\frac{\mathrm{d}G}{\mathrm{d}V} = 2\gamma\left(\frac{1}{r_2} - \frac{1}{r_1}\right) \tag{6}$$

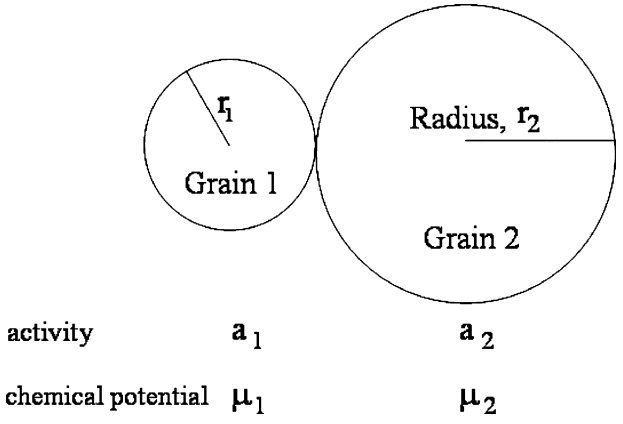

Fig. 1. A model structure of two adjacent grains with different size, activity and chemical potential.

From Eqs. (4) and (6), the difference of chemical potential is described as a function of grain size.

$$\Delta\mu = \mu_2 - \mu_1 = \upsilon\frac{\mathrm{d}G}{\mathrm{d}V} = 2\gamma\upsilon\left(\frac{1}{r_2} - \frac{1}{r_1}\right) \tag{7}$$

Eq. (7) indicates that (1) $\Delta\mu$ is 0 for an equal grain size ($r_1 = r_2$), and (2) $\Delta\mu$ is a negative value for $r_1 < r_2$. When r_2 is ∞ (flat surface), we define the μ to be μ_0. This definition leads to a general formula of Eq. (8) for the chemical potential (μ_r) of a spherical grain with radius, r.

$$\mu_\mathrm{r} = \mu_0 + \frac{2\gamma\upsilon}{r} \tag{8}$$

When a sintered microstructure consists of flat grains ($r = \infty$), all the grains have a same chemical potential (μ_0), resulting in $\Delta\mu = 0$. The chemical potential derived in Eq. (7) or (8) is related to the activity (a) of oxide ions in a grain in next section.

3. Activity of oxide ions

The activity of oxide ions (a) is related to μ by Eq. (9),

$$\mu = \mu^\bullet + RT\ln a \tag{9}$$

where $\mu^\bullet$ corresponds to the chemical potential at $a = 1$. Eq. (9) is combined with Eq. (7) to give Eq. (10).

$$\ln\left(\frac{a_2}{a_1}\right) = \frac{2\gamma\upsilon}{RT}\left(\frac{1}{r_2} - \frac{1}{r_1}\right) \tag{10}$$

When we define $a_2 = a_0$ for $r_2 = \infty$, we obtain a general form (Thomson–Freundlich equation) of the activity (a_r) of oxide ions as a function of r.

$$a_\mathrm{r} = a_0 \exp\left(\frac{2\gamma\upsilon}{RTr}\right) \tag{11}$$

The a_r is in the range of $0 \le a_\mathrm{r} \le 1$. We also obtain a useful relation (Eq. (12)) from Eq. (9) because of the relation of $\mu_0 = \mu^\bullet + RT\ln a_0$,

$$\mu_\mathrm{r} = (\mu_0 - RT\ln a_0) + RT\ln a_r \tag{12}$$

Substitution of Eq. (11) for Eq. (12) results in Eq. (8). The above relations are summarized in Table 1 as a function of grain size.

A GDC grain contains oxide ions and vacancy in its oxygen lattice sites shown in Fig. 2. The molar fraction of oxide ions, N_r, is defined using the number of oxide ions (n_r) and the total number of oxygen lattice sites ($n_\mathrm{m} = n_\mathrm{r} + n_\upsilon$, n_υ: number of oxygen vacancy) per a unit volume of spherical grain of radius r: $N_\mathrm{r} = n_\mathrm{r}/n_\mathrm{m}$. The activity of oxide ions is defined by $a_\mathrm{r} = N_\mathrm{r}\gamma^0$ and the activity coefficient γ^0 (>0) is equal to 1 for an ideal solution. The above relation is coupled with Eq. (11) to correlate the activity with the number of oxide ions in a grain of radius, r,

$$a_\mathrm{r} = \gamma^0\left(\frac{n_\mathrm{r}}{n_\mathrm{m}}\right) = a_0\exp\left(\frac{2\gamma\upsilon}{RTr}\right) = \gamma^0\left(\frac{n_0}{n_\mathrm{m}}\right)\exp\left(\frac{2\gamma\upsilon}{RTr}\right) \tag{13}$$

Table 1
Chemical potential and activity of grain with radius, r

Grain size	r = r (convex)		r = ∞ (flat)		r = − r (concave)
chemical potential (μ)	$\mu_0 + \frac{2\gamma\upsilon}{r}$	>	μ_0	>	$\mu_0 - \frac{2\gamma\upsilon}{r}$
activity (a)	$a_0 \exp\left(\frac{2\gamma\upsilon}{RTr}\right)$	>	a_0	>	$a_0 \exp\left(\frac{-2\gamma\upsilon}{RTr}\right)$

where n_0 is the number of oxide ions included in unit volume of a cubic particle ($r = \infty$). The relation in Eq. (13) leads to Eq. (14).

$$n_r = n_0 \exp\left(\frac{2\gamma\upsilon}{RTr}\right) \tag{14}$$

The condition of $a_r = 1$ in Eq. (13) leads to a critical particle size (r_c).

$$r_c = \frac{2\gamma\upsilon}{RT}\frac{1}{-\ln a_0} \tag{15}$$

Another condition for $a_r \to 0$ in Eq. (13) leads to the following relation of r: $r < 0$ and $r \to 0$. Fig. 3 shows the schematic relation for Eq. (13). The activity, $\ln a_0 < 0$, corresponds to that of flat grain of $r = \infty$. The $\ln a_r$ of a convex grain increases linearly with $1/r$ and reaches 0 ($a_r = 1$) at $r = r_c$. The $\ln a_r$ of a concave grain decreases linearly with $1/r$ to $-\infty$ at $r = 0$. Since n_r/n_m ratio in Eq. (13) is in the range from 0 to 1, the following relation is derived for $2\gamma\upsilon/RTr$ (≡Z) in Eq. (13):

$$\ln\left(\frac{n_r}{n_m}\right) = \ln\left(\frac{n_0}{n_m}\right) + Z < 0, \quad Z < -\ln\left(\frac{n_0}{n_m}\right) \tag{16}$$

From Eq. (8), the Z value is equal to $(\mu_r - \mu_0)/RT$ and represents the ratio of the difference of chemical potentials between μ_r (spherical grain) and μ_0 (flat grain) to thermal energy (RT). On the other hand, the molar fraction of oxide ions for a GDC grain of $r = \infty$ (Eq. (13)) and with a chemical composition of $Ce_{1-x}Gd_xO_{2-(x/2)}$ is calculated to be $(4 - x)/4$. From Eq. (16), Z is limited in the range of Eq. (17).

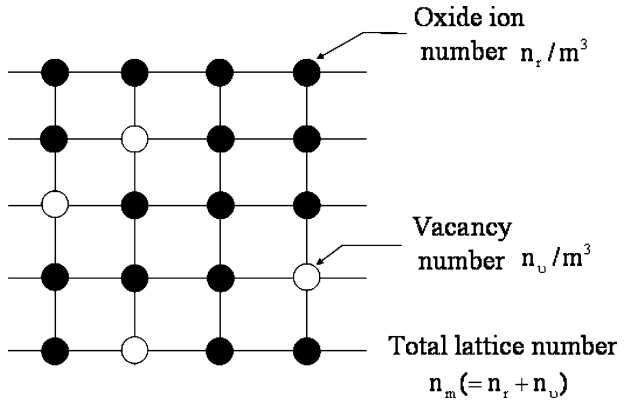

Fig. 2. A lattice model for oxide ion and vacancy.

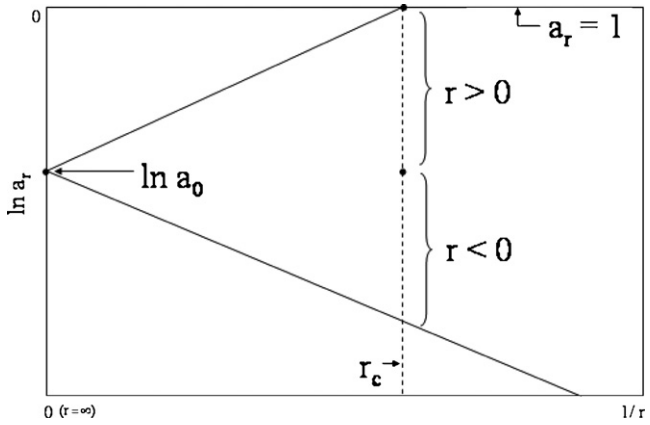

Fig. 3. Relationship between $\ln a_r$ (activity) and $1/r$ (radius) for Eq. (13) in text.

$$Z < -\ln N_0 = -\ln\left(1 - \frac{x}{4}\right) \approx \frac{x}{4} \tag{17}$$

Therefore, Z is in the range of $0 < Z < x/4 < 1/4$ for $r > 0$. Under the limited range of Z, the difference of activity for two grains in Fig. 1 is approximated to be Eq. (18) because of $\exp(Z) \approx 1 + Z (0 < Z < 0.25)$,

$$a_2 - a_1 = \gamma^0(N_2 - N_1) = a_0 \exp\left(\frac{2\gamma\upsilon}{RTr_2}\right) - a_0 \exp\left(\frac{2\gamma\upsilon}{RTr_1}\right) \approx \gamma^0 N_0 \frac{2\gamma\upsilon}{RT}\left(\frac{1}{r_2} - \frac{1}{r_1}\right) \tag{18}$$

From Eqs. (7) and (18), Eq. (19) is derived.

$$\Delta a \approx \frac{\gamma^0 N_0 \Delta\mu}{RT} \tag{19}$$

In next two sections, we correlate the difference of activity (Δa) to the flux of oxide ions at a grain boundary.

4. Flux of oxide ions at grain boundary

4.1. Description of flux of oxide ions

One-dimensional flux of oxide ions migrating under a gradient of chemical potential of oxide ions and an external electric field (ϕ) along x direction is expressed by Eq. (20) (Phenomenological equation) [17],

$$J_i = -M_i \frac{d\mu_i}{dx} - M_\phi \frac{d\phi}{dx} \tag{20}$$

where M_i and M_ϕ are constants. J_i is also equal to the product of $C_i\upsilon_i$ (C_i: concentration of migrating oxide ions, mol/L, υ_i: migration rate of oxide ions, m/s) and υ_i is related to the product of applied force F and mobility B of oxide ions. The applied force is related to the potential energy U through the equation of $F = -(\partial U/\partial x)$. The above relations are

substituted for Eq. (20),

$$J_i = C_i B_i F_i = C_i B_i \left(-\frac{\partial U}{\partial x} \right) \tag{21}$$

The potential energy of the oxide ions is represented by the electrochemical potential η_i ($=\mu_i + Z_i e\phi$, Z_i (atomic valence) is -2 for oxide ions, e the charge on electron). That is, Eq. (21) is transformed to Eq. (22),

$$J_i = -C_i B_i \left(\frac{\partial \mu_i}{\partial x} \right) - C_i B_i Z e \left(\frac{\partial \phi}{\partial x} \right) \tag{22}$$

Under no electric field, J_i is equal to $-D_i(\partial C_i/\partial x)$ as known as Fick's first law (D_i: diffusion coefficient of oxide ions) and we get the relation of Eq. (23).

$$D_i \left(\frac{\partial C_i}{\partial x} \right) = C_i B_i \left(\frac{\partial \mu_i}{\partial x} \right) \tag{23}$$

In Section 3, we derived Eq. (12) for μ_r of oxide ions in a GDC grain and activity (a_r) is related to the concentration (C) through Eq. (24),

$$a_r = \gamma^0 N_r = \gamma^0 \left(\frac{n_r}{n_m} \right) = \gamma^0 \frac{(n_r/n_A)}{(n_m/n_A)} = \gamma^0 \left(\frac{C_r}{C_m} \right) \tag{24}$$

where n_A is the Avogadro number. Therefore, $d\mu_i/dx$ in Eq. (23) for oxide ions in a grain is equal to $RT(d \ln a/dx) = RT(d \ln \gamma^0/dx) + RT(d \ln C_r/dx)$. The above relation is coupled with Eq. (23) and leads to the equation of $D_i = B_i RT(1 + (d \ln \gamma i_0/d \ln C_i))$, as known as Nernst–Einstein equation. Based on the derived above relations, we describe the flux of oxide ions at a grain boundary as follows,

$$\begin{aligned} J_i &= -D_i \left(\frac{\partial C_i}{\partial x} \right) - C_i B_i q_i \left(\frac{\partial \phi}{\partial x} \right) \\ &= -D_i \left(\frac{\partial C_i}{\partial x} \right) - \frac{D_i C_i q_i}{RThi} \left(\frac{\partial \phi}{\partial x} \right) \end{aligned} \tag{25}$$

where D_i and C_i represent the self-diffusion coefficient and concentration of oxide ions at a given grain boundary, respectively and h_i is equal to $1 + (d \ln \gamma i_0/d \ln C_i)$ and q_i is Ze ($Z = -2$). In next section, we correlate Eq. (25) to an electric current at a given grain boundary.

4.2. Electric current at grain boundary

The electric current (I_i) of oxide ions at a grain boundary is equal to the product of flux J_i and charge q_i of oxide ion and expressed by Eq. (26).

$$I_i = J_i q_i = -D_i q_i \frac{dC_i}{dx} - \frac{D_i C_i q_i^2}{RTh_i} \left(\frac{d\phi}{dx} \right) \tag{26}$$

Electric current I_i is also defined as $I_i = -\sigma_i (d\phi/dx)$, where σ_i is the grain boundary conductivity. The comparison between Eq. (26) and the definition of I_i yields Eq. (27),

$$\sigma_i = D_i q_i \left[\frac{(dC_i/dx)}{(d\phi/dx)} + \frac{C_i q_i}{RTh_i} \right] \tag{27}$$

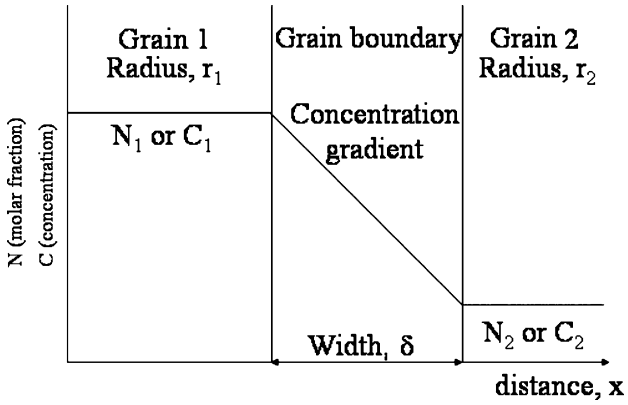

Fig. 4. Structure model of grain boundary with width δ between grain 1 and grain 2 with N_1 and N_2 molar fraction of oxide ions, respectively.

Fig. 4 shows a structure model with width δ of grain boundary between grain 1 of radius r_1 and grain 2 of radius r_2. The (dC_i/dx) in Eq. (27) is approximated to be $(C_2 - C_1)/\delta$ in this paper and C is equal to $C_m N$ (N: molar fraction of oxide ions in a grain, see Eq. (24)). Furthermore, the difference of N between two adjacent grains in Fig. 4 is given by Eq. (18). These relations lead to Eq. (28) because of $C_m N_0 = C_m(C_0/C_m) = C_0$,

$$\frac{dC_i}{dx} \approx \frac{C_2 - C_1}{\delta} = \frac{C_m N_0 2\gamma\upsilon}{\delta RT} \left(\frac{1}{r_2} - \frac{1}{r_1} \right) = \frac{C_0}{\delta} \frac{2\gamma\upsilon}{RT} \left(\frac{1}{r_2} - \frac{1}{r_1} \right) \tag{28}$$

On the other hand, the concentration of oxide ions C_i is a function of the thickness of grain boundary and depends on the concentrations of oxide ions in the adjacent two grains. However, in this paper, C_i is substituted with the average concentration ($\overline{C_i}$) for all the grain boundaries and $\overline{C_i}$ is also approximated by the average concentration $\overline{C_b}$ of oxide ions for all the grains. This approximation leads to Eq. (29) and C_i is finally related to C_0.

$$C_i \approx \overline{C_i} \approx \overline{C_b} = C_m \bar{N} = C_m N_0 = C_0 \tag{29}$$

Substitution of Eqs. (28) and (29) for Eq. (27) gives Eq. (30) as a grain boundary conductivity,

$$\begin{aligned} \sigma_i &= \frac{D_i C_0 q_i^2}{RT} \left[\frac{1}{h_i} + \frac{2\gamma\upsilon}{\delta} \left(\frac{1}{r_2} - \frac{1}{r_1} \right) \frac{1}{q_i(d\phi/dx)} \right] \\ &= \sigma_0 \left[\frac{1}{h_i} + \frac{2\gamma\upsilon}{\delta} \left(\frac{1}{r_2} - \frac{1}{r_1} \right) \frac{1}{q_i(d\phi/dx)} \right] \end{aligned} \tag{30}$$

where σ_0 represents $D_i C_0 q_i^2/RT$ for a given grain boundary. If D_i is substituted with the self-diffusion coefficient of oxide ions within a grain (D_b), σ_0 represents the bulk conductivity. The important note for Eq. (30) is that the grain boundary conductivity is mainly dominated by D_i at the grain boundary and by the difference of sizes of two adjacent grains. Further analysis is described in a latter part. Before the discussion of σ_i, we point out the important characteristics of the microstructure associated with Eq. (30).

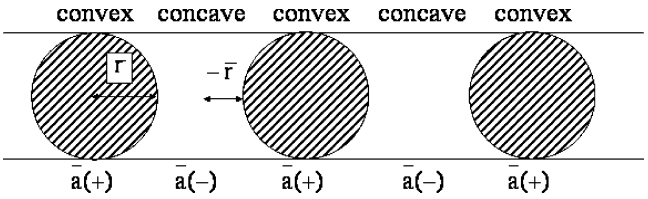

Fig. 5. One-dimensional model structure of sintered GDC, which consists of the alternative location of convex and concave grains.

The activity of oxide ions ($\overline{a_r}$) of a single crystal GDC grain of average size $\bar{r}$ is expressed as $\overline{a_r} = a_0 \exp(2\gamma\upsilon/RT\bar{r})$ (see Eq. (11)). $\overline{a_r}$ is related to the average molar fraction $\bar{N}_r$ and also related to $\overline{C_b}$ or $\bar{n}$ (average number of oxide ions in a grain): $\overline{a_r} = \gamma^0\overline{N_r} = \gamma^0\overline{C_b}/C_m = \gamma^0\overline{n_r}/n_m$. When the chemical composition of GDC is fixed, the $\bar{N}_r$ is automatically related to the composition as a constant value (see Section 3). However, $\overline{a_r}$ depends on the average grain size $\bar{r}$ and is not treated as a constant value. The above discrepancy for $\overline{a_r}$ is solved by analyzing the microstructure of sintered GDC. Fig. 5 shows one-dimensional model structure of sintered GDC. In this model, convex and concave grains are alternatively located. The activity of convex ($\bar{a}(+)$) and concave ($\bar{a}(-)$) grains with size of $\bar{r}$ is given by Eqs. (31) and (32), respectively.

$$\bar{a}(+) = a_0 \exp\left(\frac{2\gamma\upsilon}{RT\bar{r}}\right) \tag{31}$$

$$\bar{a}(-) = a_0 \exp\left(-\frac{2\gamma\upsilon}{RT\bar{r}}\right) \tag{32}$$

The product of $\bar{a}(+)\,\bar{a}(-)$ is equal to a_0^2 for the grains of $r = \infty$ (cubic grain). That is, the overall average activity ($\bar{a}(\pm)$) for the sintered microstructure is expressed by Eq. (33).

$$\bar{a}(\pm) = \sqrt{\bar{a}(+)\bar{a}(-)} = a_0 \tag{33}$$

Eq. (33) indicates that (i) it is impossible to form a sintered microstructure by only convex or only concave grains with average size $\bar{r}$, (ii) a sintered microstructure consists of the alternative location of convex and concave grains and (iii) the overall average activity ($\bar{a}(\pm)$) results in a constant value a_0 which is correlated to the composition of GDC. When we discuss the grain boundary conductivity, the requirement from the microstructure should be included.

4.3. Detailed analysis of grain boundary conductivity

Based on Eq. (30), we discuss the relationship between the local microstructure of sintered GDC and grain boundary conductivity. *Case A. Equal grain size*: When the two convex grains shown in Fig. 1, have a same grain size, the σ_i at the interface is equal to σ_0/h_i in Eq. (30) because of $r_2 = r_1$ and is independent of the electric field. *Case B. Flat grain structure (cubic grain)*: In Eq. (30), the condition of $r_1 = r_2 = \infty$ results in $\sigma_i = \sigma_0/h_i$. This result is same as Case A. *Case C. Convex grain with radius r_1 and convex grain with radius r_2 ($r_1 < r_2$)*: Fig. 6 shows the schematic relation between the structure of two grains and direction of electric field. The term $(1/r_2 - 1/r_1)$ is

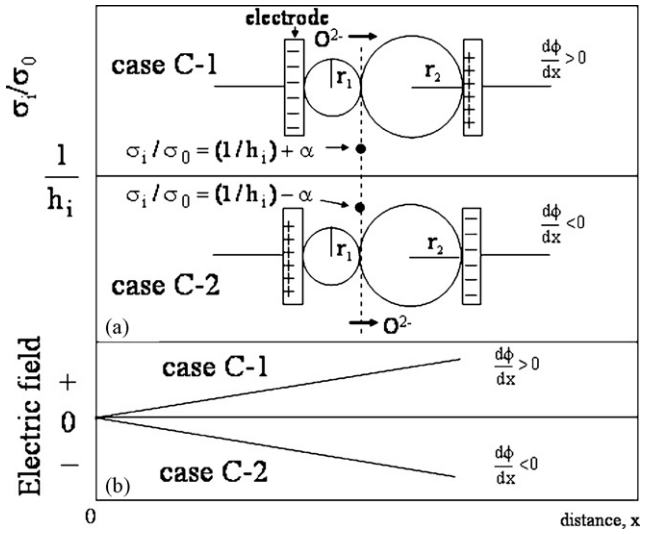

Fig. 6. Relation among (a) structure of two grains, (b) direction of electric field and σ_i/σ_0 ratio of Eq. (30) in text.

negative and q_i (for oxide ion) is also negative. Under the condition of $d\phi/dx > 0$, the ratio of σ_i/σ_0 becomes greater than $1/h_i$. When the term of $|2\gamma\upsilon(1/r_2 - 1/r_1)/\delta q_i(d\phi/dx)|$ is expressed by α, the ratio σ_i/σ_0 increases to $(1/h_i) + \alpha$. This result indicates that the migration of oxide ions from small grain to large grain through the grain boundary is enhanced by the application of external electric field. On the contrary, σ_i/σ_0 decreases to $(1/h_i) - \alpha$ for $d\phi/dx < 0$. This result indicates that the migration of oxide ions from small grain to large grain is suppressed by the influence of negative electric field. The difference of grain sizes and the direction of electric field affect the grain boundary conductivity. When the location of grain 1 and grain 2 is exchanged, a similar result is obtained: $\sigma_i/\sigma_0 = (1/h_i) - \alpha$ for $d\phi/dx > 0$ and $\sigma_i/\sigma_0 = (1/h_i) + \alpha$ for $d\phi/dx < 0$. Case D: alternative location of convex and concave grains with same size ($\bar{r}$) For the microstructure shown in Fig. 5, r_1 is changed to $\bar{r}$ and r_2 is changed to $-\bar{r}$ in Eq. (30). As a result, Eq. (30) is written as Eq. (34).

$$\frac{\sigma_i}{\sigma_0} = \frac{1}{h_i} + \left|\frac{2\gamma\upsilon}{\delta}\frac{2}{\bar{r}}\frac{1}{q_i(d\phi/dx)}\right| \tag{34}$$

The second term of right equation is treated as β in this paper. Fig. 7 shows the relationship between the microstructure and normalized conductivity (σ_i/σ_0). A care should be placed on σ_0 in Eqs. (30) and (34). The D_i in σ_0 depends on the direction of given grain boundary and D_i for the migration of oxide ions is different between the two directions: from convex to concave grains and from concave to convex grains. Here, the former D_i and σ_0 are written $D_i(+)$ and $\sigma_0(+)$, respectively, and $D_i(-)$ and $\sigma_0(-)$ are also written for latter case. The σ_i/σ_0 (+) ratio increase to $(1/h_i) + \beta$ for the migration of oxide ions from convex to concave direction at the grain boundary under the condition of $d\phi/dx > 0$. On the contrary, the $\sigma_i/\sigma_0(-)$ ratio decreases to $(1/h_i) - \beta$ for the migration of oxide ions from concave to convex direction under the condition of $d\phi/dx > 0$. Similarly, the migration of oxide ions from concave to convex direction is

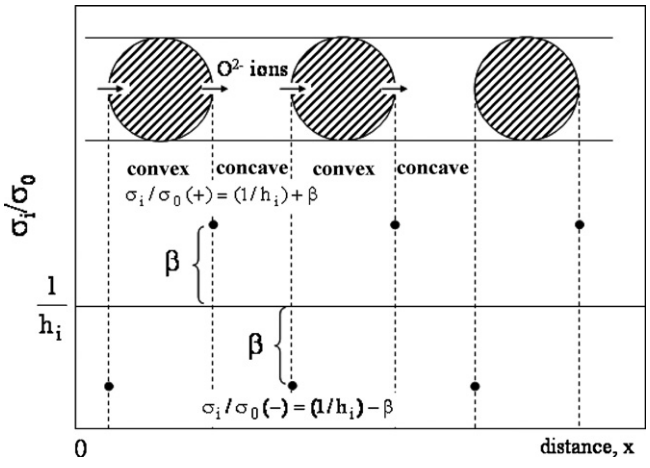

Fig. 7. One-dimensional microstructure and σ_i/σ_0 ratio in Eq. (30) for $d\phi/dx > 0$.

enhanced to $\sigma_i/\sigma_0(-) = (1/h_i) + \beta$ at $d\phi/dx < 0$. The migration of oxide ions from convex to concave is reduced to $\sigma_i/\sigma_0(+) = (1/h_i) - \beta$ at $d\phi/dx < 0$. As shown in Fig. 7, the enhancement and suppression occur alternatively for the migration of oxide ions at the two grain boundaries under a given electric field.

We discuss more about Eq. (34). Fig. 8 shows the relationship between σ_i/σ_0 ratio and $1/\bar{r}$ for a constant value of $d\phi/dx$ (>0). A linear relation is proposed between the σ_i/σ_0 and $1/\bar{r}$. As discussed in Section 3, the grain size has a critical minimum value of r_c which corresponds to $a_r = 1$ (Eq. (15)). The grain boundary conductivity reaches a maximum value at $\bar{r} = r_c$: $\sigma_i/\sigma_0(+)(\text{maximum}) = 1 + 2RT \ln a_0/\delta q_i (d\phi/dx)$ ($-\ln a_0 < 0$, $q_i < 0$). On the other hand, $\sigma_i/\sigma_0(-)$ decreases with an decrease of grain size. When $-\bar{r}$ of concave grain reaches $-r_c$, $\sigma_i/\sigma_0(-)$ reaches a minimum value of $\sigma_i/\sigma_0(-) = (1/h_i) - 2RT \ln a_0/\delta q_i (d\phi/dx)$. In the grain size $r_c > \bar{r}$, no change of σ_i/σ_0 (+) or $\sigma_i/\sigma_0(-)$ with grain size occurs. In the above grain size range, $\bar{a}(+)$ is unity and the corresponding $\bar{a}(-)$ results in a constant value of a_0^2 from Eq. (33). This constant values of $\bar{a}(+)$ and $\bar{a}(-)$ give a constant flux of oxide ions between two adjacent grains, which is independent of grain size (see Eq. (18)).

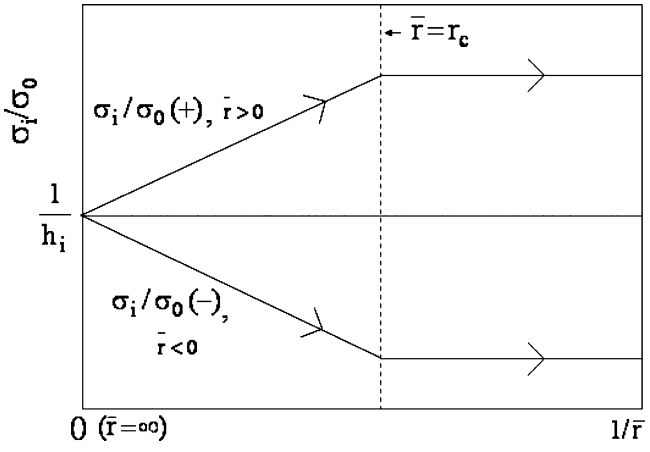

Fig. 8. Relationship between σ_i/σ_0 ratio and $1/\bar{r}$ of Eq. (34) for $d\phi/dx > 0$.

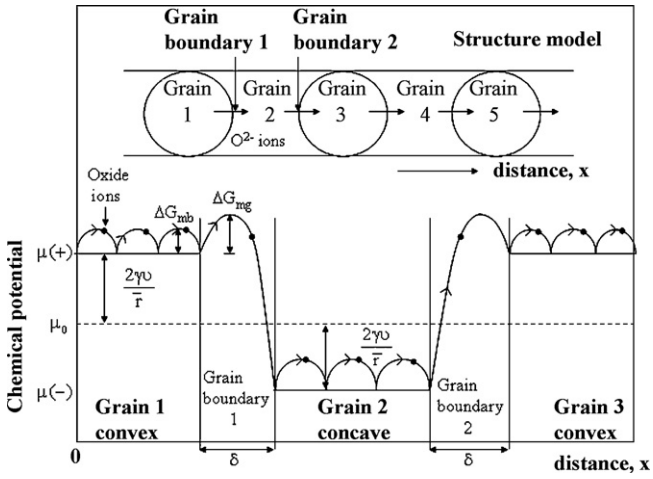

Fig. 9. One-dimensional model structure and corresponding chemical potential of oxide ions in convex and concave grains as a function of distance, x. The grain boundary is drawn to have a width of δ. The dotted line of μ_0 represents the chemical potential of oxide ions in flat grains. The $\mu(+)$ and $\mu(-)$ represent two chemical potential of oxide ions in convex and concave grains, respectively. The schematic curve shows the jump of oxide ions in the potential barrier.

4.4. Dependence of activation energy of grain boundary conductivity on grain size

Based on the sintered microstructure model shown in Fig. 5, we analyze the activation energy of grain boundary conductivity. Fig. 9 shows the chemical potential of oxide ions in the adjacent two grains forming a grain boundary. The convex grain has a high chemical potential of $\mu_0 + 2\gamma\upsilon/\bar{r}$ (see Eq. (8)) and the chemical potential of the adjacent concave grain is low, $\mu_0 - 2\gamma\upsilon/\bar{r}$. The oxide ions within a single crystal grain need a certain activation energy (ΔG_{mb}) to diffuse into an adjacent oxygen vacancy. This activation energy represents the summation of energies for migration of oxygen vacancy and association of oxygen vacancy and dopant ion [18–20]. The size and concentration of dopant affect ΔG_{mb}. Similarly, an activation energy (ΔG_{mg}) is generally needed for the oxide ions within the convex grain (high chemical potential) to diffuse to the oxygen vacancy within an adjacent concave grain (low chemical potential) through the grain boundary. On the other hand, the oxide ions within the concave grain (low chemical potential) can diffuse to convex grain (high chemical potential) when the ions get a high energy of $\Delta G_{mg} + (4\gamma\upsilon/\bar{r})$. This potential barrier apparently depends on the average grain size and becomes higher for smaller grain size. The self-diffusion coefficient, D_i, in Eq. (30) is expressed by Eqs. (35) and (36) for the oxide ion flux from convex to concave grain ($D(+)$) and from concave to convex grain ($D(-)$), respectively.

$$D(+) = D_0(+)\exp\left(-\frac{\Delta G_{mg}}{RT}\right) \tag{35}$$

$$D(-) = D_0(-)\exp\left(-\frac{\Delta G_{mg} + ((4\gamma\upsilon)/\bar{r})}{RT}\right) \tag{36}$$

when $\bar{r}$ is ∞, $D(+)$ is equal to $D(-)$, indicating the both the frequency factors are equal ($D_0(+) = D_0(-) = D_0(\pm)$). Eqs. (35)

Table 2
Grain boundary conductivity parameters l and m in Eq. (39)

No.	Direction of migration of oxide ions	l	m
1	Convex → concave	0	–4
2	Convex → flat	0	–2
3	Flat → concave	0	–2
4	Flat → flat	0	0
5	Flat → convex	+2	+2
6	Concave → flat	+2	+2
7	Concave → convex	+4	+4
8	Concave → concave	0	0
9	Convex → convex	0	0

and (36) are substituted for Eq. (34) to present the corresponding conductivity.

$$\sigma_i(+) = \frac{C_0 q_i^2 D_0(\pm)}{RT}\exp\left(-\frac{\Delta G_{mg}}{RT}\right)\left[\frac{1}{h_i} - \frac{4\gamma\upsilon}{\delta\bar{r}}\frac{1}{q_i(\mathrm{d}\phi/\mathrm{d}x)}\right] \quad (37)$$

$$\sigma_i(-) = \frac{C_0 q_i^2 D_0(\pm)}{RT}\exp\left(-\frac{(\Delta G_{mg} + (4\gamma\upsilon/\bar{r}))}{RT}\right) \times \left[\frac{1}{h_i} + \frac{4\gamma\upsilon}{\delta\bar{r}}\frac{1}{q_i(\mathrm{d}\phi/\mathrm{d}x)}\right] \quad (38)$$

The grain boundary conductivity for another type interface structure, for example convex grain → flat grain, flat grain → concave grain, flat grain → flat grain, is also analyzed. The derived general form of σ_i is expressed by Eq. (39).

$$\sigma_i = \frac{C_0 q i_2 D_0(\pm)}{RT}\exp\left(-\frac{\left(\Delta G_{mg} + l\gamma\upsilon/\bar{r}\right)}{RT}\right) \times \left[\frac{1}{hi} + \frac{m\gamma\upsilon}{\delta\bar{r}}\frac{1}{qi(\mathrm{d}\phi/\mathrm{d}x)}\right] \quad (39)$$

The values l and m for $q_i = -2e$ (oxide ions) are summarized in Table 2. The variety of the diffusion of oxide ions in Table 2 comes from the complex structure of sintered GDC as shown in Fig. 10, which should satisfy the condition of $\bar{a}(\pm) = a_0$ (see Eq. (33)). The small l value indicates the low energy barrier for the diffusion of oxide ions through a grain boundary. As seen in Fig. 9, the diffusion of oxide ions from a high chemical potential grain to a low chemical potential grain or diffusion between grains of same chemical potential results in $l = 0$. For example, the condition for $\bar{r} = \infty$ in Eq. (36) indicates the diffusion of oxide ions between flat grains and gives the activation energy of ΔG_{mg}. The large negative m value shows the large enhancement effect for the diffusion of oxide ions at the grain boundary. Fig. 11 shows the potential barrier associated with l value in Table 2. In the proposed grain

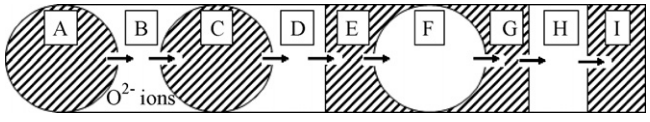

Fig. 10. A typical complex structure associated with the variety of migration of oxide ions through possible interfaces.

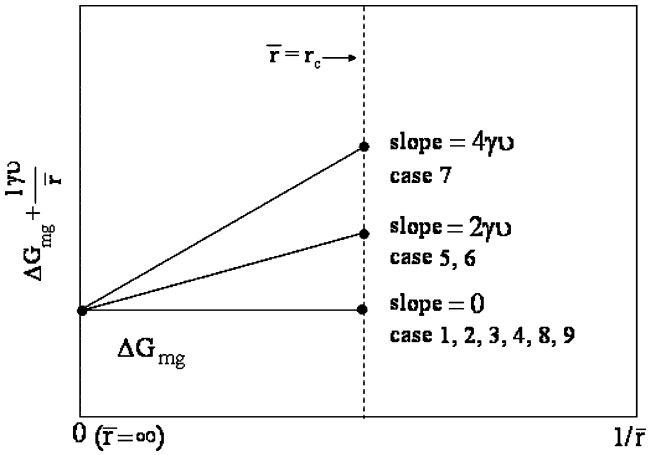

Fig. 11. Potential barrier associated with l value in Table 2.

boundary model, three types of potential barrier appear. In cases 1, 2, 3, 4, 8 and 9 for $l = 0$ in Table 2, the potential barrier is same and independent of the grain size. In cases 5, 6 and 7, the potential barrier increases with decreasing grain size. At the grain size r_c, σ_i results in a maximum value in cases 5, 6 and 7. The potential barrier at $\bar{r} = r_c$ is $(\Delta G_m/RT) + (l\gamma\upsilon/RT\bar{r}) = (\Delta G_m/RT) + (lZ/2) < (\Delta G_m/RT) + (lx/8)$ ($Z = (2\gamma\upsilon/RTr) < x/4$, see Eq. (17)), where x is the molar fraction of Gd substituted for Ce in $Ce_{1-2}Gd_xO_{2-(x/2)}$. The $l\,RT\,x/8$ value is 0.48 kJ/mol at 573 K for $l = 4$ and $x = 0.2$. On the other hand, the reported activation energy of grain boundary conductivity, which corresponds to $\Delta H_m + (l\gamma\upsilon/\bar{r})$, is 83.6–112 kJ/mol. This magnitude is significantly large as compared with the ($l\,RT\,x/8$) value. Therefore, the activation energy of grain boundary conductivity is not sensitive to the average grain size.

The total conductivity (σ_t) for the microstructure shown in Fig. 5 is expressed by Eq. (40) from Eqs. (37) and (38),

$$\sigma(t) = \frac{1}{2}[\sigma_i(+) + \sigma_i(-)] = \frac{1}{2}\sigma_0(\pm)\left[\frac{1}{h_i} + \beta + \left(\frac{1}{h_i} - \beta\right)\exp\left(-\frac{4\gamma\upsilon}{RT\bar{r}}\right)\right] \quad (40)$$

where $\sigma_0(\pm)$ represents $(C_0 q_i^2 D_0(\pm)\exp(-\Delta G_{mg}/RT)/RT)$ in Eq. (37) or (38) and β is equal to $|4\gamma\upsilon/\delta\,\bar{r}q_i(\mathrm{d}\phi/\mathrm{d}x)|$. Since $(4\gamma\upsilon/RT\bar{r})$ is smaller than 0.5 (see Eq. (17)), $\exp(-4\gamma\upsilon/RT\bar{r})$ is approximated to be $1 - (4\gamma\upsilon/RT\bar{r})$. The $4\gamma\upsilon/RT$ is also equal to $2r_c u$, where u represents $(-\ln a_0)$ (see Eq. (15)). In addition, $|RT/\delta q_i(\mathrm{d}\phi/\mathrm{d}x)|$ is written as b. The above substitution is carried out on Eq. (40) to express $\sigma(t)$ as a function of $r_c/\bar{r}(\equiv y)$ ratio. The obtained equation is

$$\frac{\sigma(t)}{\sigma_0(\pm)} = \frac{1}{h_i} - \frac{u}{h_i}y + 2bu^2y^2 = 2bu^2\left(y - \frac{1}{4buh_i}\right)^2 + \frac{1}{h_i} - \frac{1}{8b}\frac{1}{h_i^2} \quad (41)$$

Fig. 12 shows a typical calculation of Eq. (41) for $h_i = 1$, $b = 0.208$, $u = 0.0513$. The $\sigma(t)/\sigma_0(\pm)$ ratio shows a small

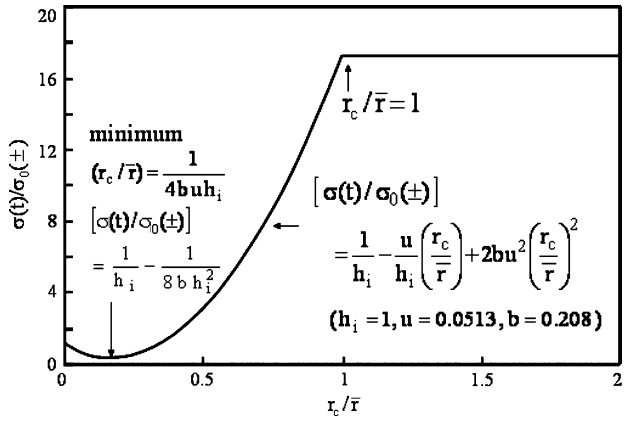

Fig. 12. Typical calculation of total conductivity ($\sigma(t)$) expressed by Eq. (41) as a function $r_c/\bar{r}$ ratio.

minimum value $(1/h_i - (1/8bh_i^2))$ at $y = 1/4buh_i$, and increases nonlinearly and reaches $(1/h_i) - (u/h_i) + 2bu^2$ at $y = 1$. In the range of $y > 1$, the $\sigma(t)/\sigma_0(\pm)$ becomes a constant value, because the activity $\bar{a}(+)$ and $\bar{a}(-)$ is fixed to be 1 and a_0^2, respectively. That is, the decrease of grain size of GDC is greatly effective to increase the grain boundary conductivity but this effect stops at the critical grain size r_c corresponding to $\overline{a_r} = 1$. Of cause, a similar analysis for another type of local microstructure (Fig. 10) is possible using the relation presented in Table 2.

5. Comparison between the theory and experimental results of grain boundary conductivity

The finally derived conductivity model (Eq. (41)) and Fig. 12 are compared with the conductivity for $Ce_{0.8}Gd_{0.2}O_{1.9}$ (GDC) reported by Christie and Berkel [12] and by our group [21]. The ac impedance method was used to separate the bulk resistance and grain boundary resistance of sintered GDC in an average size rang from 290 nm to 17 μm. The detailed

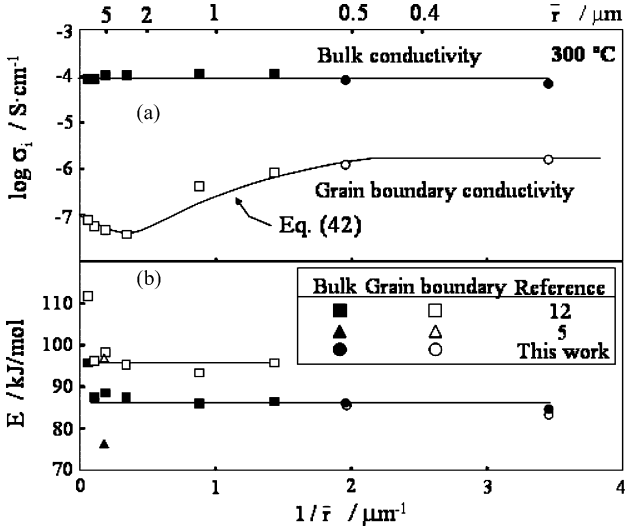

Fig. 13. Grain boundary conductivity and bulk conductivity (a) and their activation energies (b) for $Ce_{0.8}Gd_{0.2}O_{1.9}$ as a function of reciprocal grain size.

experimental procedure is described in the original papers [5,7,12]. The observation of GDC with grains of average size 5.6 μm by high-resolution transmission electron microscopy indicated that no crystalline or amorphous secondary phase formed in the bulk or grain boundaries [6]. Fig. 13 shows the separated bulk and grain boundary conductivity at 300 °C in air and the corresponding activation energy measured in the temperature range of 300–800 °C. When the heating temperature is increased above 500 °C, it is difficult to separate the conductivity because of the small resistance of the grain boundary conduction. The logarithmic grain boundary conductivity as a function $1/\bar{r}$ shows a minimum value at $\bar{r} = 2.94\ \mu m$ and gradually increases with decreasing grain size. On the other hand, the data for the grain sizes of 290 and 510 nm, which were recently measured in our group [21], were almost independent of grain size. The described characteristics agreed with the prediction from the theory in Section 4.4. Eq. (41) is transformed into Eq. (42) and this equation is fitted to the measured data.

$$\sigma(t) = \sigma_0(\pm)\left[\left(\frac{1}{h_i}\right) - \left(\frac{ur_c}{h_i}\right)\left(\frac{1}{\bar{r}}\right) + (2bu^2r_c^2)\left(\frac{1}{\bar{r}}\right)^2\right]$$
$$= \sigma_0(\pm)\left[2bu^2r_c^2\left(\frac{1}{\bar{r}} - \frac{1}{4bur_ch}\right)^2 + \frac{1}{h_i} - \frac{1}{8bh_i^2}\right] \quad (42)$$

From the comparison of the theoretical curve and experimental results, the following value were determined for both the experiments by Christie and Berker, and our group: $r_c = 0.47$ μm and $u(= -\ln a_0) = 7.07$. The corresponding activation energy is shown in Fig. 13(b). Although the slight difference was recognized between the data of the two research groups, the important characteristic is the small grain size dependence of the activation energy (E). This result is also well explained by the theory in 4.4 and the E value extrapolated at $1/\bar{r} = 0$ represents the enthalpy term of ΔG_{mg} in Eq. (39). From the above comparison between the theory and experimental results, it is concluded that the grain boundary conductivity of oxide ions of GDC can be characterized by Eqs. (39) and (41) and the r_c corresponding to $a_r = 1$ sets a limit to the increased conductivity with decreasing grain size.

Here we note the importance of activity in Eq. (15). The experimentally determined a_0 was 8.50×10^{-4} for the data in Fig. 13(a). On the other hand, the N_0 value ($=1 - (x/4)$, x is the molar fraction of oxide ions in $Ce_{0.8}Gd_{0.2}O_{1.9}$, $x = 0.2$) is 0.95. Both the values are correlated by the activity coefficient γ^0:

$a_0\ (=8.50 \times 10^{-4}) = N_0\ (=0.95)\ \gamma^0$, $\gamma^0 = 8.95 \times 10^{-4}$ at 300 °C. This result indicates that (1) the activity of oxide ions is far small as compared with the molar faction N_0 and (2) the oxide ions cannot be treated as an ideal solution at this temperature. As shown in Eq. (15), the product $(-\ln a_0)\ r_c$ is a function of temperature ($(-\ln a_0)\ r_c = 2\gamma\upsilon/RT$. We know experimentally the value of product $(-\ln a_0)\ r_c$ and r_c value at each heating temperature. In a next paper, we study the temperature dependence of a_0 and r_c.

Fig. 13 shows also the bulk conductivity at 300 °C and the activation energy for the diffusion oxide ions within a grain. In

this paper, we discussed briefly the diffusion of oxide ions in a grain in Section 4.2. As seen in Fig. 13(a), the bulk conductivity in the wide grain size range shows a constant value. Although no information about the grain size of GDC is described in Ref. [20], the reported sample conductivity ($\sigma_t = 1.26 \times 10^{-4}$ S cm^{-1}) at 300 °C is very close to the bulk conductivity in Fig. 13(a). The sintered GDC contains a series of grain size distribution and each grain has a different activity of oxide ions. However, the overall average activity is related to the composition of GDC and independent of grain size (see Eq. (33)). No change of the bulk conductivity with the average grain size is well explained by the constant composition of GDC. The activation energy for the bulk conductivity in Fig. 13(b) shows a constant value with decreasing grain size and close to the activation energy of grain boundary conductivity measured by our group [21]. Although no grain size of GDC was presented in Ref. [19], the activation energy of 75.3 kJ/mol was measured for their sample conductivity. On the other hand, Balazs and Glass [22] reported the activation energy of 85.8 kJ/mol for the sample conductivity of GDC with grains of 5–30 μm sizes. These values are also comparable to the data shown in Fig. 13(b). The similar activation energy and relatively large difference of conductivity between bulk and grain boundary suggest that the pre-exponential factor D_0 (Eq. (39)) of self-diffusion coefficient for bulk is significantly larger than that for grain boundary. The more discussion about D_0 will be studied in a next paper.

6. Conclusions

In this paper, we correlated the activity (a_r) and chemical potential (μ_r) of oxide ions within a single crystal grain of Gd-doped ceria with a curvature, r. The migration of oxide ions through a grain boundary between adjacent two grains was analyzed under a given gradient of chemical potentials of oxide ions and a given external electric field. The theoretically derived conclusions are as follows. An overall average activity $\bar{a}(\pm)$ of oxide ions within grains is equal to the activity a_0 for $r = \infty$ (cubic grain). This conclusion indicates that a sintered microstructure consists of alternative location of convex and concave grains. The microstructure has a critical grain size (r_c) for $a_r = 1$. The diffusion of oxide ions from high activity grain (convex) to low activity grain (concave) through the grain boundary (written as $\sigma_i(+)$) is accelerated under a positive electric field. On the contrary, the migration of oxide ions from low activity grain (concave) to high activity grain (convex) through the grain boundary (written as $\sigma_i(-)$) is suppressed by the applied positive electric field. The opposite phenomenon occurs for the negative electric field. The electrical conductivity (σ_i) increases or decreases linearly with increasing $1/r$, depending on the characteristics of the grain boundary. However, σ_i becomes a constant value at $r_c > r$ because of $a_r = 1$ ($r > 0$) or $a_r = a_0^2$ ($r < 0$) in this grain size range. The activation energy for the migration of oxide ions depends on the difference of chemical potential of adjacent two grains and is a function of grain size for the migration of oxide ions from low activity grain to high activity grain. However, this influence of grain size on the activation energy is as small as ~0.5 kJ/mol in the wide grain size range from r_c to ∞ at 573 K. The total conductivity $\sigma(t) = [\sigma(+) + \sigma(-)]/2$ is theoretically expressed by a curve of second degree of reciprocal grain size ($1/r$) and reaches a maximum value at $r = r_c$. Under the condition of $r_c > r$, $\sigma(t)$ becomes a constant value because of the fixed activity of convex and concaved grains. The derived theory was compared with experimentally measured grain boundary conductivity. The grain size dependence of measured $\sigma(t)$ and activation energy was in accordance with the theory.

References

[1] Y. Hirata, S. Yokomine, S. Sameshima, Y. Shimonosono, S. Kishi, H. Fukudome, Electrochemical properties of solid fuel cell with Sm-doped ceria electrolyte and cermet electrodes, J. Ceram. Soc. Japan 113 (9) (2005) 597–604.

[2] G. Hiramatu, Y. Hirata, S. Sameshima, N. Matsunaga, Electrochemical properties of perovskite cathode for solid oxide fuel cell, Mater. Sci. Forum 544–545 (2007) 985–988.

[3] M. Nagamori, Y. Hirata, S. Sameshima, Influence of hydrogen sulfide in fuel on electric power of solid oxide fuel cell, Mater. Sci. Forum 544–545 (2007) 997–1000.

[4] T. Shimonosono, X.H. Wang, G. Hiramatsu, Y. Hirata, S. Shamesima, N. Matsunaga, T. Doi, T. Horita, Electrochemical properties of cathode for solid oxide fuel cell, Key Eng. Mater. 352 (2007) 255–258.

[5] Y. Hirata, H. Ono, K. Higashi, K. Sonoda, S. Sameshima, Y. Ikuma, Microstructure and electrical conductivity of rare earth-doped ceria, in: S.K. Sundaram, D.F. Bickford, E.J. Hornyak, Jr. (Eds.), Ceramic Transactions, vol. 92, Electrochemistry of Glass and Ceramics, The American Ceramic Society, Westerville, OH, 1999, pp. 137–148.

[6] S. Sameshima, H. Ono, K. Higashi, K. Sonoda, Y. Hirata, Microstructure of rare earth-doped ceria prepared by oxalate coprecipitation method, J. Ceram. Soc. Japan 108 (11) (2000) 985–988.

[7] S. Sameshima, H. Ono, K. Higashi, K. Sonoda, Y. Hirata, Y. Ikuma, Electrical conductivity and diffusion of oxygen ions in rare earth-doped ceria, J. Ceram. Soc. Japan 108 (12) (2000) 1060–1066.

[8] T. Shimonosono, Y. Hirata, Y. Ehira, S. Sameshima, T. Horita, Electronic conductivity measurement of Gd- and Sm-doped ceria ceramics by Hebb–Wagner Method, J. Ceram. Soc. Japan 112 (5) (2004) S616–S621.

[9] T. Shimonosono, Y. Hirata, Y. Ehira, S. Sameshima, T. Horita, H. Yokokawa, Electronic conductivity measurement of Sm- and La-doped ceria ceramics by Hebb–Wagner Method, Solid State Ionics 174 (2004) 27–33.

[10] T. Shimonosono, Y. Hirata, S. Sameshima, T. Horita, Electronic conductivity of La-doped ceria ceramics, J. Am. Ceram. Soc. 88 (8) (2005) 2114–2120.

[11] R. Gerhardt, A.S. Nowick, Grain boundary effect in ceria doped with trivalent cations. I. Electrical measurements, J. Am. Ceram. Soc. 69 (9) (1986) 641–646.

[12] G.M. Christie, F.P.F. van Berkel, Microstructure-ionic conductivity relationships in ceria-gadolinia electrolytes, Solid State Ionics 83 (1996) 17–27.

[13] T. Mori, T. Kobayashi, Y. Wang, J. Drennan, T. Nishimura, J.G. Li, H. Kobayashi, Synthesis and characterization of nano-hetero-structured by doped CeO_2 solid electrolytes using a combination of spark plasma sintering and conventional sintering, J. Am. Ceram. Soc. 88 (7) (2005) 1981–1984.

[14] N. Sakai, Y.P. Xiong, K. Yamaji, H. Yokokawa, Y. Terashi, H. Seno, Anomalous conductivity and microstructure in gadolinium doped ceria prepared from nano-sized powder, Solid State Ionics 177 (2006) 2503–2507.

[15] D.R. Ou, T. Mori, F. Ye, T. Kobayashi, J. Zou, G. Auchterlonie, J. Drennan, Oxygen vacancy ordering in heavily rare earth-doped ceria, Appl. Phys. Lett. 89 (17) (2006) 1911–1913.
[16] R.H. Doremus, Rates of Phase Transformations, Academic Press, Inc., Orland, FL, 1985, pp. 149–157.
[17] P.G. Shewmon, Diffusion in Solids, McGrew-Hill Book Company, New York, 1963, pp. 115–163.
[18] J. Feber, C. Geoffroy, A. Roux, A. Sylvestre, P. Ablard, A systematic investigation of the dc electrical conductivity of rare earth doped ceria, Appl. Phys. A 49 (1989) 225–232.
[19] B.C.H. Steele, Appraisal of $Ce_{1-y}Gd_yO_{2-y/2}$ electrolytes for IT-SOFC operation at 500 °C, Solid State Ionics 129 (2000) 95–110.
[20] M. Mogensen, N. Sammes, G. Tompsett, Physical, chemical and electrochemical properties of pure and doped ceria, Solid State Ionics 129 (2000) 63–94.
[21] A. Hara, Y. Hirata, S. Sameshima, N. Mastunaga, T. Horita, Grain size dependence of electrical properties of Gd-doped ceria, J. Ceram. Soc. Japan 116 (2008) 291–297.
[22] G.B. Balazs, R.S. Glass, AC impedance studies of rare earth oxide doped ceria, Solid State Ionics 76 (1995) 155–162.